JOURNAL OF MATERIALS SCIENCE 21 (1986) 1139–1144

Influence of pressure and crystallization rate on the surface microhardness of high-density polyethylene

F. J. BALTÁ CALLEJA, D. R. RUEDA, J. GARCIA PEÑA
Instituto de Estructura de la Materia, CSIC, Serrano 119, Madrid 6, Spain
F. P. WOLF*, V. H. KARL
Fritz-Haber Institut der MPG, Berlin, Dahlem, Germany

The indentation microhardness *MH* of high-density polyethylene crystallized at different pressures p and crystallization rates v_c has been investigated. The results confirm that *MH* is an increasing function of lamellar thickness and therefore of density ϱ. The rate of increase depends on the crystallization conditions p and v_c. Crystallization at high pressure leads to *MH* values considerably higher than those of samples prepared under atmospheric pressure. The results are discussed in terms of compressed amorphous regions contributing to an elastic release after removal of the indenter. For samples crystallized under different pressures the hardness value turns out to be nearly independent of the elastic modulus E. For samples crystallized at different rates v_c there is a steady decrease of microhardness with increasing v_c (decrease of lamellar thickness) but no simple relationship with E. With higher rates v_c the appearance of strained tie molecules provokes a rapid increase of E while *MH* decreases further because the crystals become smaller.

1. Introduction

Indentation microhardness (*MH*) has been shown to be a bridging parameter between the bulk properties of polymer materials (density ϱ, elastic modulus E and yield stress y) on one side and microstructural parameters (crystal thickness l and unit cell cross-section) on the other [1–3]. In the case of semicrystalline polymers like polyethylene the degree of crystallinity x_c and the superstructural arrangement of the constituent units (hard crystalline and compliant amorphous regions) play an important role in determining the *MH* value. In addition, the superstructural arrangement of these units can be modified by orientation through plastic deformation of the material, leading to substantial changes of the microhardness values [4–8]. In the case of isotropic materials [1–3] the microstructural parameters were mainly controlled by using a series of samples with varying number of chain defects (branching, unsaturation) and molecular weights, leading to large differences in ϱ, E and *MH*. Even if one uses identical starting materials, a considerable hardening has been achieved through annealing treatment and controlled acid exposure of the polymer material [9–11].

The purpose of the present investigation is to extend the above studies to measurements of *MH*, ϱ and E for samples of high-density polyethylene (HDPE) crystallized from the melt under different conditions of pressure and crystallization rate, and to relate these data to microstructural parameters. We will show that changes of *MH* of more than 30% can be produced on the same polymer material just by varying the crystallization conditions, and that the hardening obtained can lead to *MH* values close to those of metals and alloys like lead or lead–antimony. This work is related to previous studies on the influence of preparation conditions of melt-crystallized HDPE on the bulk elastic modulus E and density ϱ of the material [12, 13].

2. Experimental details

2.1. Material and sample preparation

A commercial linear polyethylene (Lupolen 6041D of BASF, Ludwigshafen, FRG) with $\bar{M}_w = 2 \times 10^5\,g\,mol^{-1}$ and a wide molecular weight distribution was used. The degree of branching is $< 0.1\%$. After crystallization under atmospheric pressure the density is $\varrho = 0.965$ to $0.967\,g\,cm^{-3}$. The melting temperature measured at low heating rate ($< 1\,K\,h^{-1}$) is $T_m = 136°\,C$.

The samples were prepared in the shape of cylindrical bars (length $\simeq 80\,mm$, diameter $\simeq 8\,mm$) by compression moulding. The inclusion of air bubbles was avoided by evacuating the mould cavity after filling with the polymer pellets. When the polymer material was melted, pressure was applied axially from one side by means of a piston. One series of samples was prepared at different pressures varying in equidistant steps between $p = 14.9$ and $148.7\,MN\,m^{-2}$ at a constant cooling rate of $1.14\,K\,min^{-1}$. This procedure

Present address: Berliner Elektronenspeichering-Gesellschaft für Synchrotron-Strahlung (BESSY), Berlin, Germany.

0022–2461/86 $03.00 + .12

corresponds to a crystallization rate of $v_c = 1.1 \times 10^{-3}\,\mathrm{sec}^{-1}$ (see Table I below). A second series of samples was prepared under a constant pressure of $p = 148.7\,\mathrm{MN\,m}^{-2}$ at different rates of crystallization between $v_c = 0.06 \times 10^{-3}$ and $28.7 \times 10^{-3}\,\mathrm{sec}^{-1}$ (see Table II). The slower rates were verified by non-isothermal crystallization at varying cooling rates between 0.05 and $3.6\,\mathrm{K\,min}^{-1}$, whereas for higher rates isothermal pressure-induced crystallization was used. The crystallization rate v_c (the reciprocal of the crystallization half-time) was derived from the volume curves as a function either of temperature or time during the crystallization process [14–16].

In the case of non-isothermal crystallization at constant cooling rate the volume of the molten polymer at the beginning of the crystallization and the volume of the solid sample at 75° C were used as reference points to measure the volume change. From the cooling rate and the temperature difference between the beginning and half of the volume change the half-time of crystallization was obtained.

In the case of isothermal crystallization the sudden pressure increase provokes an instant volume decrease of the melt. This point offers an upper reference for the volume change during crystallization. The time between the start and half of the volume change was read directly from the volume against time curve.

2.2. Measurement techiques

All measurements of MH, E and ϱ were performed at room temperature $T \simeq 22°\,\mathrm{C}$ and atmospheric pressure. Density ϱ was determined from the geometrical dimensions and the mass of the samples.

Elastic modulus E was evaluated from longitudinal resonant vibrations at extremely small stresses and strains (the latter of the order of 10^{-7}) of the samples in their fundamental modes and their first overtones at frequencies of about 10 and 20 kHz, respectively [12, 13]. For the material crystallized under atmospheric pressure ($0.1\,\mathrm{MN\,m}^{-2}$) the dynamically measured elastic modulus is $E_{dyn} = 3000\,\mathrm{MN\,m}^{-2}$. In order to compare these data with moduli derived from quasi-static measurements, both the true and the nominal stress–strain curves of this material were obtained at room temperature and atmospheric pressure up to 800% elongation [17]. Fig. 1 shows that the nominal stress σ_0 reaches its maximum value of $30\,\mathrm{MN\,m}^{-2}$ at 10% elongation (yield point), then decreases to about $15\,\mathrm{MN\,m}^{-2}$ and finally slowly increases up to $24\,\mathrm{MN\,m}^{-2}$ without failure of the sample. The ultimate strength is larger than this value. The true stress σ_w, of course, increases continuously up to a value of about $240\,\mathrm{MN\,m}^{-2}$ (which is 1/4 the strength value obtained for steel) for the highly drawn material. The values for the nominal stress and strain were recorded by using an Instron testing machine with a strain gauge in 0.08% steps of longitudinal strain. For the evaluation of true stresses σ_w an additional strain gauge was attached to measure the diameter of the sample during straining. For strains below that of the yield point there is no significant difference between σ_0 and σ_w. The elastic modulus E can, then, be evaluated directly as so-called secant modulus according to Hooke's law.

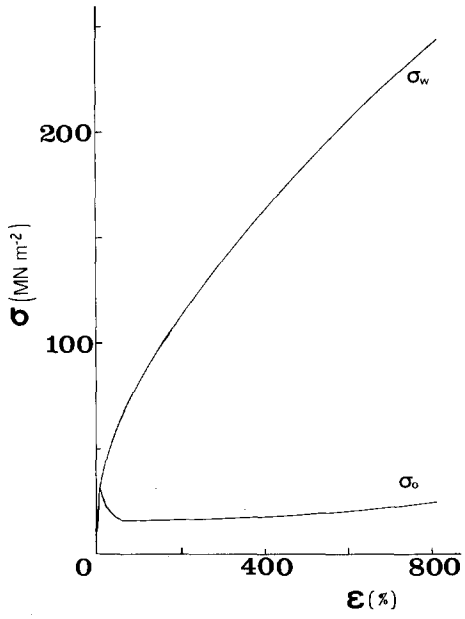

Figure 1 Nominal stress σ_0 and true stress σ_w against strain ε for melt-crystallized high-density polyethylene (Lupolen 6041 D).

Fig. 2 shows the variation of E as a function of strain. At 1% strain this curve yields a value of $E_{stat} = 1300\,\mathrm{MN\,m}^{-2}$. This value corresponds to the dynamically determined value $E_{dyn} = 3000\,\mathrm{MN\,m}^{-2}$ at 10 kHz, as mentioned above. For ease of comparison with earlier published data we decided to convert all the dynamically measured values E_{dyn} into quasi-static moduli, E, at 1% elongation by means of the relation $E = 1300/3000\ E_{dyn}$ [12, 13]. Since all measurements were performed at room temperature one may presume that the frequency dispersion between E_{dyn} and E_{stat} should not change considerably with pressure and rate of crystallization.

The microhardness MH was measured using a Leitz Tester with a square pyramid indenter. MH was calculated fom the residual projected area according to

$$MH = K\frac{P}{d^2} \tag{1}$$

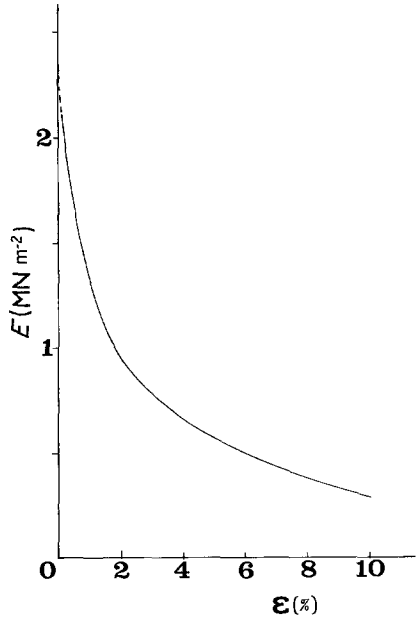

Figure 2 Dependence of elastic modulus E, evaluated from secants in Fig. 1, on strain ε.

TABLE I Properties of polyethylene as a function of crystallization pressure p at a constant crystallization rate v_c

Sample No.	Crystallization pressure p (MN m^{-2})	Density ϱ (g cm^{-3})	Microhardness MH (MN m^{-2})	Elastic modulus E (MN m^{-2})	Crystallization rate v_c (10^{-3} sec^{-1})	Crystallinity x_c (%)	Long period L (nm)	Crystal thickness l (nm)
0	0.1	0.9670	73.5	1300	$\gg 1$	79.0	35.2	27.8
1	14.9	0.9674	80.4	1284	1.10	79.3		
2	29.7	0.9678	81.8	1310	1.10	79.5	37.3	29.6
3	44.6	0.9685	83.0	1320	1.10	80.0		
4	59.5	0.9689	89.2	1319	1.10	80.3		
5	74.4	0.9688	93.9	1333	1.10	80.2	37.3	29.9
6	89.2	0.9692	95.1	1328	1.10	80.8		
7	104.1	0.9699	95.7	1356	1.10	80.9		
8	119.0	0.9699	101.2	1327	1.10	80.9	37.3	30.2
9	133.8	0.9704	100.6	1354	1.10	81.3		
10	148.7	0.9705	100.9	1360	1.10	81.3	37.3	30.3

where d is the length of the indentation diagonal, P the contact load applied and K a geometrical factor equal to 1.854. The hardness is taken here as indicative of the irreversible deformation processes characterizing the material. Loads of 0.15 and 0.5 N were employed to eliminate the instant elastic contribution. A loading cycle of 6 sec was used.

The small-angle X-ray scattering (SAXS) patterns for some of the samples of the two series were obtained with a Rigaku camera using point collimation and an 8 kW rotating anode X-ray source. Nickel-filtered Cu$K\alpha$ radiation was used. The photographs were taken with the beam perpendicular to both the direction of applied pressure and the surface of the X-ray film. The long period L was calculated from Bragg's equation from the first maximum of scattering intensity after subtraction of the background. The crystal thickness l was approximated from $l = Lx_c$. Crystallinity x_c was derived from density measurements according to

$$x_c = \frac{\varrho_c [(\varrho - \Delta\varrho_f) - \varrho_a]}{(\varrho - \Delta\varrho_f)(\varrho_c - \varrho_a)} \quad (2)$$

with $\varrho_a = 0.868\,\mathrm{g\,cm^{-3}}$ and $\varrho_c = 1000\,\mathrm{g\,cm^{-3}}$. The actual density ϱ of the sample was corrected for the influence of internal stresses due to the crystallization conditions [13] by a small amount $\Delta\varrho_f \approx 0.002 - 0.006\,\mathrm{g\,cm^{-3}}$.

3. Results

Crystallization pressure p, density ϱ, microhardness MH, elastic modulus E, crystallization rate v_c, crystallinity x_c, long period L and crystal thickness l are collected for two series of samples in Tables I and II. Fig. 3 illustrates the gradual increase of MH as a function of crystallization pressure from 73.5 MN m^{-2} for $p = 0.1$ up to 101 MN m^{-2} for the highest pressure used, $p \simeq 150\,\mathrm{MN\,m^{-2}}$. An extrapolation of these values to pressures above 500 MN m^{-2} (typical for the extended-chain morphology [18]) is consistent with the calculated microhardness value $H_c = 150$ to 170 MN m^{-2} derived from the cohesive energy density based on Van der Waals forces of an ideal polyethylene crystal [19]. The MH values of samples crystallized at about 150 MN m^{-2} are approximately 25% higher than those of samples crystallized at atmospheric pressure. As can be seen from Table I the changes of E ($\sim$4.6%) under these conditions are considerably smaller.

Fig. 4 illustrates the gradual decrease of MH with increasing crystallization rate v_c, showing a larger decreasing tendency for $v_c > 5 \times 10^{-4}\,\mathrm{sec^{-1}}$. The density data in Table II show the same decreasing behaviour whereas the modulus E only decreases for values $v_c < 10^{-2}\,\mathrm{sec^{-1}}$, while for values of $v_c > 10^{-2}\,\mathrm{sec^{-1}}$, E increases.

The samples of Table I (v_c = const) show an SAXS pattern in the form of a halo giving a long period of $\sim$37.3 nm which remains practically constant with increasing p. The samples crystallized at constant pressure (Table II) yield, on the contrary, an SAXS pattern which varies substantially with crystallization rate (Fig. 5). In addition to the notable decrease of

TABLE II Properties of polyethylene as a function of crystallization rate v_c at constant crystallization pressure p

Sample No.	Crystallization pressure p (MN m^{-2})	Density ϱ (g cm^{-3})	Microhardness MH (MN m^{-2})	Elastic modulus E (MN m^{-2})	Crystallization rate v_c (10^{-3} sec^{-1})	Crystallinity x_c (%)	Long period L (nm)	Crystal thickness l (nm)
11	148.7	0.9785	111.3	1570	0.06	84.3		
12	148.7	0.9770	110.3	1461	0.15	83.0		
13	148.7	0.9758	110.3	1440	0.31	82.0	45.7	37.5
14	148.7	0.9740	108.9	1392	0.52	80.5		
15	148.7	0.9723	105.6	1353	1.10	79.0	37.3	29.5
16	148.7	0.9710	96.5	1316	1.83	77.8		
17	148.7	0.9700	97.9	1332	2.64	76.9	35.2	27.1
18	148.7	0.9677	97.1	1288	9.10	74.9	32.4	24.2
19	148.7	0.9658	88.0	1515	19.6	73.2	32.4	23.7
20	148.7	0.9633	79.5	1661	26.2	71.0	30.8	21.8

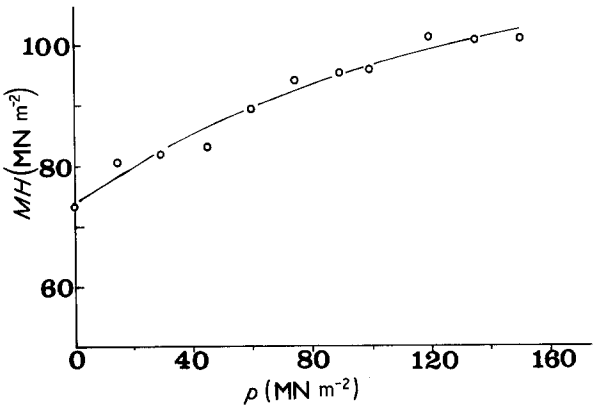

Figure 3 Microhardness MH against crystallization pressure p.

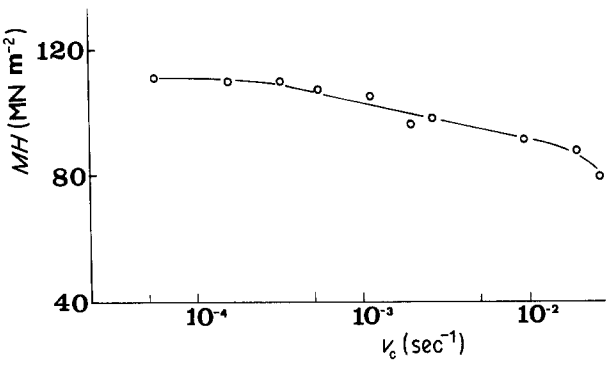

Figure 4 Microhardness MH against crystallization rate v_c.

long period L given in Table II one observes a gradual change from a nearly uniform scattering ring at low crystallization rates into a first-order meridional maximum at high crystallization rates. That means that the lamellae tend to orientate normal to the direction of the applied pressure, especially for $v_c \geqslant 10^{-2}\,\mathrm{sec}^{-1}$. When total lamellar orientation is reached one observes an upturn of elastic modulus E (Samples 19 and 20 in Table II).

4. Discussion

Crystal hardness H_c has been shown to be a function of the cohesion energy ϕ_e of the material [20]. Since the overall microhardness MH depends on the packing of the molecules both within the crystalline and amorphous phases (which in turn determines the density of the bulk material) it seems justifiable to analyse MH as a function of ϱ for the samples under investigation as we have done previously [2, 3]. Fig. 6 shows that there is a strong upward trend of MH with increasing density ϱ (the straight line marked I). There is good agreement between the values of Sample No. 0 of this investigation and former measurements on samples also prepared under atmospheric pressure (broken line [3]). With increasing pressure one obtains now a much steeper increase of MH with ϱ (I) than on the broken line. The plot of MH against ϱ for the second series of samples, crystallized at varying crystallization rates, shows on the other hand, a curve (II) with a smaller slope and a tendency to level off for high density (low crystallization rate). The fit between Curves I and II for $p \simeq 150\,\mathrm{MN\,m}^{-2}$ and $v_c \simeq 10^{-3}\,\mathrm{sec}^{-1}$ is good, and enables us to separate the independent influence of both parameters, p and v_c, on MH.

In order to correlate the polymer microhardness MH with microstructural parameters the material can be visualized as a composite consisting of hard (crystalline) and soft (amorphous) elements. The hardness of such a system has been approximated [2, 19] to

$$MH = X_c H_c + (1 - X_c) H_a \qquad (3)$$

where H_c and H_a are the hardness values for the crystals and the amorphous layers, respectively. Since $H_c \gg H_a$ ($H_c \gtrsim 170\,\mathrm{MN\,m}^{-2}$ and $H_a \sim 0.5\,\mathrm{MN\,m}^{-2}$),

$$MH \sim X_c H_c \qquad (4)$$

Fig. 7 illustrates the plot of H_c against the reciprocal of crystal thickness for the samples crystallized at $p \simeq 150\,\mathrm{MN\,m}^{-2}$ (Table II). The data are in consonance with the thermodynamically predicted relationship between H_c and l^{-1} given [21] by

$$H_c = \frac{H_0 \Delta\phi^*}{(1 + b_1 l^{-1})} \qquad (5)$$

where H_0 is a constant and $\Delta\phi^*$ is the work per unit volume performed during indentation. For $l \to \infty$, H_c approaches $H_0\Delta\phi^*$, which is the maximum possible value of dissipated energy through local plastic deformation. For polyethylene [19] $H_0\Delta\phi^* \simeq 170$ MN m^{-2}. For samples crystallized at $p \simeq 150\,\mathrm{MN\,m}^{-2}$ a constant $b_1 = 10\,\mathrm{nm}$ in Equation 5 provides a good fit with the experimental results, while for

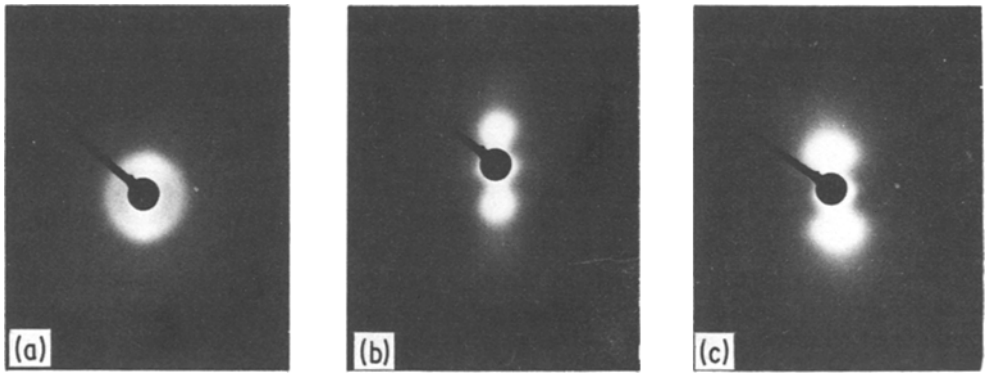

Figure 5 SAXS patterns of polyethylene crystallized at $p \simeq 150\,\mathrm{MN\,m}^{-2}$ and v_c = (a) $2.64 \times 10^{-3}\,\mathrm{sec}^{-1}$, (b) $9.10 \times 10^{-3}\,\mathrm{sec}^{-1}$, (c) $26.2 \times 10^{-3}\,\mathrm{sec}^{-1}$.

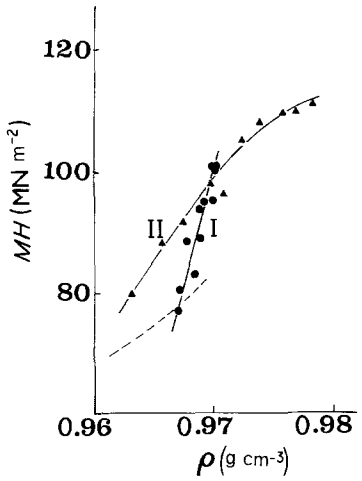

Figure 6 Microhardness MH against density ϱ for the samples of (●) Table I a and (▲) Table II; dotted line from data of Martinez Salazar and Baltá Calleja [3].

materials crystallized under atmospheric pressure a value of $b_1 \simeq 20\,\text{nm}$ is required. The data for H_c with increasing p (Table I) shown in Fig. 7 cover the range for Equation 5 from $b = 20\,\text{nm}$ to $b_1 = 10\,\text{nm}$ for $l^{-1} \sim 33$ to $33.8 \times 10^{-3}\,\text{nm}^{-1}$, and confirm the view that pressure enhances the H_c value and consequently depresses the b_1 parameter in Equation 5.

In Fig. 8 the elastic modulus E is plotted against the microhardness MH for both series of samples. Application of pressure during crystallization markedly enhances the MH values (Line I), but increases E only slightly. It is well known that crystallization under pressure leads to a lamellar thickening which according to Equation 5 enhances the crystal hardness H_c (and consequently the overall hardness MH). However, the data for $p \simeq 150\,\text{MN m}^{-2}$ as represented in Fig. 7 suggest that an additional hardening mechanism is involved. We have previously suggested [12] that due to the different values of compressibility of the amorphous and crystalline regions in partially crystalline polyethylene, the amorphous phase after releasing the pressure is still compressed to some extent ("internal pressure").

The enhanced density of the amorphous regions due to this compression hardly influences the elastic modulus E, because E is measured by means of tensile stress and strain. The indentation process, on the other hand, involves local compressive stresses and deformations, and the amorphous regions of enhanced density (i.e. under the influence of internal pressure) are less compressible than the relaxed amorphous material. Since three-dimensional compression entails an elastic deformation of the material, the elastic recovery after load removal, at the end of the indentation cycle, is larger for samples with internally compressed amorphous regions. An elastic recovery would result in an apparently enhanced microhardness MH, as compared with samples prepared under atmospheric pressure. This MH enhancement leads to an apparent increase of H_c of some 25% for a crystallization pressure of $p \simeq 150\,\text{MN m}^{-2}$ as shown in Fig. 7.

The decrease of MH obtained with increasing crystallization rate (Fig. 4) can easily be explained in terms of the decreasing crystal thickness l as illustrated in Fig. 5 and Table II, and justified by the predictions of Fig. 7. The situation with the elastic modulus E is somewhat more complex. For low crystallization rates (high MH values) the increase of E from 1300 to almost $1600\,\text{MN m}^{-2}$ is explained by the increase of lamellar thickness and the higher degree of crystallinity. The slow crystallization process entails relaxing tie molecules so that E is governed by the series arrangement of crystalline and relaxed amorphous layers [22]. At high crystallization rates, on the contrary, we obtain a strong increase of E from 1300 to more than $1650\,\text{MN m}^{-2}$, and a concurrent decrease of MH from 100 to $80\,\text{MN m}^{-2}$. This antagonism between E and MH can only be understood on the basis of a larger number of strained tie molecules acting between adjacent crystals at high crystallization rates [13]. Hence E increases with the number of strained molecules at the lamellar interfaces, while MH diminishes with decreasing crystal size and crystallinity for large v_c values.

5. Conclusions

In summary, the microhardness of melt-crystallized

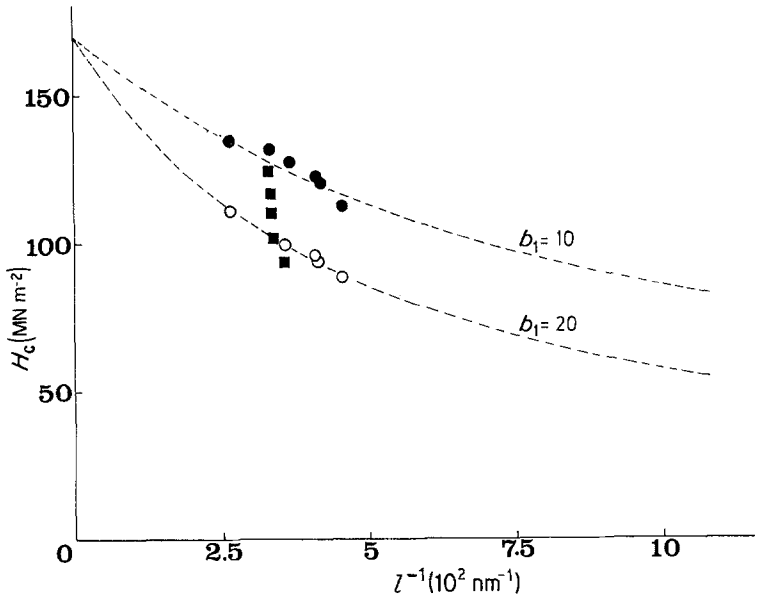

Figure 7 Crystal hardness H_c against reciprocal of lamellar thickness l^{-1} for polyethylene according to Equation 5. (●) Data from samples crystallized at $p \sim 150\,\text{MN m}^{-2}$, and (○) values reduced for atmospheric pressure (see text). (■) Data from samples crystallized at different pressures (Table I).

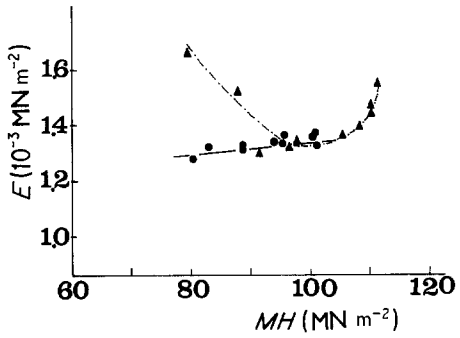

Figure 8 Elastic modulus E against microhardness MH for the samples of (●) Table I and (▲) Table II.

linear high-density polyethylene can be considerably increased by two different routes. One way is by means of lamellar thickening and increase of crystallinity by applying slow crystallization rates, whereby ϱ and E are augmented concurrently. The other route is to crystallize the material under high pressure, leading to a partially compressed amorphous phase accompanied by comparatively small increases in E and ϱ. It is suggested that the hardness increase in this material crystallized at high pressure entails a substantial elastic contribution. Furthermore, the increase of E with decreasing MH for the rapidly crystallized samples indicates that there is no unequivocal relationship between these two quantities, and that the preparation conditions even for one selected material play a decisive role.

Acknowledgement

Thanks are due to CAICYT, Spain, for the support of this investigation.

References

1. F. J. BALTÁ CALLEJA, *Colloid Polym. Sci.* **254** (1976) 258.
2. F. J. BALTÁ CALLEJA, J. MARTINEZ SALAZAR, H. CACKOVIC and J. LOBODA-CACKOVIC, *J. Mater. Sci.* **16** (1981) 739.
3. J. MARTINEZ SALAZAR and F. J. BALTÁ CALLEJA, *ibid.* **18** (1983) 1077.
4. F. J. BALTÁ CALLEJA and D. C. BASSETT, *J. Polym. Sci.* **C58** (1977) 157.
5. F. J. BALTÁ CALLEJA, D. R. RUEDA, R. S. PORTER and W. T. MEAD, *J. Mater. Sci.* **15** (1980) 765.
6. D. R. RUEDA, F. J. BALTÁ CALLEJA and R. K. BAYER, *ibid.* **16** (1981) 3371.
7. D. R. RUEDA, F. J. BALTÁ CALLEJA and P. F. VAN HUTTEN, *J. Mater. Sci. Lett.* **1** (1982) 496.
8. D. R. RUEDA, F. J. BALTÁ CALLEJA, J. G. PEÑA, I. M. WARD and A. RICHARDSON, *J. Mater. Sci.* **19** (1984) 2615.
9. D. R. RUEDA, J. MARTINEZ SALAZAR and F. J. BALTÁ CALLEJA, *ibid.* **20** (1985) 834.
10. J. MARTINEZ SALAZAR, D. R. RUEDA, M. E. CAGIAO, E. LÒPEZ CABARCOS and F. J. BALTÁ CALLEJA, *Polym. Bull.* **10** (1983) 553.
11. F. J. BALTÁ CALLEJA, C. FONSECA, J. M. PERÉÑA and J. G. FATOU, *J. Mater. Sci. Lett.* **3** (1984) 509.
12. V. H. KARL and F. P. WOLF, *Angew. Makromol. Chem.* **79** (1979) 21.
13. F. P. WOLF and V. H. KARL, *ibid.* **79** (1979) 37.
14. V. H. KARL, F. ASMUSSEN and K. UEBERREITER, *ibid.* **62** (1977) 145.
15. V. H. KARL, *Kunststoffe* **68** (1978) 247.
16. F. P. WOLF, *Prog. Coll. Polym. Sci.* **64** (1978) 195.
17. F. P. WOLF and J. MEIER, *Colloid Polym. Sci.* **260** (1982) 762.
18. D. C. BASSETT, in "Principles of Polymer Morphology" (Cambridge University Press, Cambridge, 1981) p. 167.
19. F. J. BALTÁ CALLEJA, *Adv. Polym. Sci.* **66** (1985) 117.
20. J. MARTINEZ SALAZAR, J. G. PEÑA and F. J. BALTÁ CALLEJA, *Polym. Commun.* **26** (1985) 57.
21. F. J. BALTÁ CALLEJA and H. G. KILIAN, *Colloid Polym. Sci.* **263** (1985) 697.
22. H. G. KILIAN, *ibid.* **262** (1984) 374.

Received 24 October 1984
and accepted 30 May 1985